

# Hermite coordinate interpolation kernels: application to image zooming

Konstantinos K. Delibasis<sup>a,\*</sup>, Iro Oikonomou<sup>b</sup>, Aristides I. Kechriniotis<sup>c</sup>, Georgios N. Tsigaridas<sup>d</sup>

<sup>a</sup>Department of Computer Science and Biomedical Informatics, University of Thessaly, 2-4 Papasiopoulou str., P.O. 35131 Lamia, Greece

<sup>b</sup>Department of Informatics and Telecommunications, National and Kapodistrian University of Athens, Panepistimioupolis, Ilisia 157 84, Athens Greece

<sup>c</sup>Department of Physics, University of Thessaly, 3rd Km Old National Road Lamia–Athens 35100, Lamia Greece

<sup>d</sup>Department of Physics School of Applied Mathematical and Physical Sciences, National Technical University of Athens, Zografou Campus GR-15780 Zografou, Athens Greece

---

## Abstract

A number of basic image processing tasks, such as any geometric transformation require interpolation at subpixel image values. In this work we utilize the multidimensional coordinate Hermite spline interpolation defined on non-equal spaced, rectilinear grids and apply it to a very common image processing task, image zooming. Since Hermite interpolation utilizes function values, as well as partial derivative values, it is natural to apply it to image processing tasks as a special case of equi-spaced grid, using numerical approximations of the image partial derivatives at each pixel. Furthermore, the task of image interpolation requires the calculation of image values at positions with nono-zero fractional part. Thus, any spline interpolation can be written as convolution with an appropriate kernel. In this context we generate the Hermite kernels according to the derived  $n$ -dimensional interpolant of Theorem 2 in [1]. We show that despite the increased complexity of the interpolant, once the kernels are constructed, the Hermite spline interpolation can be applied to images as efficiently as any other less complicated method. Finally, we perform illustrative numerical examples to showcase the applicability and high accuracy of the proposed Hermite kernels for image zooming, compared to other interpolation methods, both traditional convolution-based, as well as employing deep learning, in terms of PSNR, as well as SSIM error metrics. The proposed Hermite spline kernels outperform all other methods in the majority of the test images, in experiments using many cascaded repetitions of the zoom operation. Interesting conclusions can be drawn considering all methods under comparison.

**Keywords:** polynomial image interpolation, multivariate Hermite, Hermite spline kernels, image zoom

---

## 1. Introduction

Any image geometric transformation requires image values at new, non-integer positions. The classic approach to this task is to employ an interpolation method using the given image values at neighboring pixels, as support points. Since any image consists of hundreds or even thousands of lines and columns, every image interpolation method is implemented as splines, piece-wise continuous polynomial functions defined over a small number of support points (image pixels), to maintain a low degree.

---

\*Corresponding author. Tel.: (+30) 22310 66908.

URL: kdelibasis@gmail.com (Konstantinos K. Delibasis), iro.oikonomou99@gmail.com (Iro Oikonomou), arisk7@gmail.com (Aristides I. Kechriniotis), gtsig@mail.ntua.gr (Georgios N. Tsigaridas)

In this work, we utilize the definition of splines based on Hermite polynomials on  $n$ -dimensional grids, [1], to define  $n$ -dimensional Hermite spline convolution kernels. Hermite interpolation has been proposed for signal and image applications [12], [2] achieving very competitive results, however these implementations were based on Theorems specifically for 1D and 2D, not easily generalizable to higher dimensions, whereas they did not consider spline construction, thus their execution was slow. The construction of Hermite kernels greatly accelerates the execution of Hermite interpolation, which otherwise would be of increased arithmetic complexity. In general, for any interpolation technique using kernel  $K(\mathbf{x}_0)$ , the value of an ( $n$ -dimensional) image  $I$  at a non-integer location  $\mathbf{x}_0$  (assuming integer pixel coordinates) is obtained as  $I(\mathbf{x}_0) = \sum_{\mathbf{a}} I(\mathbf{a})K(\mathbf{x}_0 - \mathbf{a})$ , which is the discrete convolutional summation.

Let us consider the case of 2D image scaling by integer factor  $s$ , hereforth referred as zooming. In this very common geometric transformation, the fractional parts of the unknown image positions are constant. I.e., in the special case of  $s = 2$ , for each given image pixel  $(i, j) = (x, y)$ , the new image values have to be computed at three new locations:  $(x+0.5, y)$ ,  $(x, y+0.5)$ ,  $(x+0.5, y+0.5)$ . Since any interpolation kernels depends on the fractional part of the required point, interpolation is most efficiently implemented by pre-constructing three different kernels  $K_{10}^H, K_{01}^H, K_{11}^H$  and convolving the image with each one to generate the values at the intermediate points to the right, south and south-east of each of the initial image pixels, respectively. Figure 7 depicts this process graphically using green squares for the given pixels and red, blue and yellow circles for the east, south and south-east pixels, respectively. This is a generic approach, applicable to any convolution-based method and it is considered computationally very efficient, since image convolution operations are implemented in highly parallelizable manner.

The rest of the paper is structured as follows. The  $n$ -dimensional Hermite spline is presented in Theorem 2.4. The generic Hermite kernel is constructed in section 4. The specific task of x2 image zoom is expressed as image interpolation task that requires only 3 kernels (by any convolution-based image interpolation method, one of them being the proposed  $n$ -dimensional Hermite spline).

We experiment with different settings of the Hermite splines, namely the support point stencil  $3 \times 5$  and  $3 \times 3$  pixels, as well as the order of the image partial derivatives up to 2nd and 3rd order for each spatial dimension. We also explore the image derivative approximation and we include the Hermite kernel and the necessary derivative kernels into a single kernel, which further accelerates the execution and results in a very simple implementation. We also construct the corresponding kernels from other state-of-the-art interpolation methods, including the generalized convolution ones (maximal order minimal support- OMOMS- and b-splines), and we further include a few established super-resolution methods based on Deep learning. Comparative results are finally presented for real world image datasets.

## 2. The proposed Hermite interpolation on $n$ -D rectilinear grids

### 2.1. Introduction and Notations of Hermite interpolation

This work focuses on multivariate classical Hermite interpolation with support points arranged on an  $n$ -dimensional non-equally spaced rectilinear grid ( $nD$  grid), given the value of a function, as well as its derivatives up to an arbitrary maximum order, defined independently for each point and each dimension.

Let  $A$  be a set,  $|A|$  the cardinality of  $A$ , and  $A^n := A \times \cdots \times A$ . Given the sets  $A_1, \dots, A_n$ , then  $\mathbf{A} := A_1 \times \dots \times A_n$ . Further, the element  $(a_1, \dots, a_n) \in \mathbf{A}$  will be denoted by  $\mathbf{a}$ . Let  $\mathbf{0} = (0, 0, \dots, 0)$ ,  $\mathbf{1} = (1, 1, \dots, 1)$  be the zero vector and ones vector, respectively. Thus, points  $\mathbf{a} = (a_1, \dots, a_n)$  are arranged on a non-regular  $N$ -dimensional grid  $\mathbf{A}$ . Let  $\mathbb{k}$  be a field of characteristic zero. For  $\mathbf{a} \in \mathbb{k}^n$ , and  $\mathbf{m} \in \mathbb{N}_0^n$  we denote  $\mathbf{a}^{\mathbf{m}} := \prod_{i=1}^n a_i^{m_i}$ . Let  $\mathbf{k} = (k_1, \dots, k_n)$  be an  $n$ -dimensional vector of non-negative integers, holding the order of partial derivatives of the interpolating polynomial with respect to each variable.

In  $\mathbb{N}_0^n$  we define the relation " $\leq$ " as follows:  $\mathbf{k} \leq \mathbf{m}$  if and only if  $k_i \leq m_i$ , for every  $i = 1, \dots, n$ . Clearly  $(\mathbb{N}_0^n, \leq)$  is a poset ( $\mathbb{N}_0^n$  is partially ordered). If  $\mathbf{k} \leq \mathbf{m}$  and  $\mathbf{k} \neq \mathbf{m}$ , then  $[\mathbf{k}, \mathbf{m}] := \{\mathbf{l} \in \mathbb{N}_0^n : \mathbf{k} \leq \mathbf{l} \leq \mathbf{m}\} = [k_1, m_1] \times \cdots \times [k_n, m_n]$ , and is valid  $||[\mathbf{k}, \mathbf{m}]|| = \prod_{i=1}^n (m_i - k_i + 1)$ .

Given the finite subsets  $A_i$ ,  $i = 1, \dots, n$  of the field  $\mathbb{k}$ , and the multiplicity functions  $\nu_i : A_i \rightarrow \mathbb{N}$ ,  $i = 1, \dots, n$ . Then for  $i \in \{1, \dots, n\}$ , and  $a_i$  any element of  $A_i$ , we define

$$H_{a_i}(x_i) := \prod_{\substack{c \in A_i \\ c \neq a_i}} \left( \frac{x_i - c}{a_i - c} \right)^{v_i(a)} \in \mathbb{K}[x_i]. \quad (2.1)$$

Let  $\nu : \mathbf{A} \rightarrow \mathbb{N}^n$  be the generalized multiplicity function given by  $\nu(\mathbf{a}) := (\nu_1(a_1), \dots, \nu_n(a_n))$ . For  $\mathbf{a} \in \mathbf{A}$  and  $\mathbf{k} \in [\mathbf{0}, \nu(\mathbf{a}) - \mathbf{1}]$  we define

$$H_{(\mathbf{a}, \mathbf{k})}(x_1, \dots, x_n) := \prod_{i=1}^n \frac{(x_i - a_i)^{k_i} H_{a_i}(x_i)}{k_i!} \in \mathbb{K}[x_1, \dots, x_n]. \quad (2.2)$$

We define the partial derivative operator acting on  $f$  as

$$\partial^{\mathbf{k}} := \prod_{i=1}^n \partial_i^{k_i}, \quad \partial_{\mathbf{a}}^{\mathbf{k}} f(\mathbf{x}) := \partial^{\mathbf{k}} f(\mathbf{x})|_{\mathbf{x}=\mathbf{a}}, \quad \text{where } \partial_i^k := \frac{\partial^k}{\partial x_i^k}.$$

The article is organized as follows. Having defined some necessary notations, we provide in the next section the...

**Remark 1.** It is easy to verify that

$$\left| \left\{ \mathbf{a}^{\mathbf{k}} : \mathbf{a} \in \mathbf{A}, \mathbf{k} \in [\mathbf{0}, \nu(\mathbf{a}) - \mathbf{1}] \right\} \right| = \sum_{\mathbf{a} \in \mathbf{A}} \sum_{\mathbf{k} \in [\mathbf{0}, \nu(\mathbf{a}) - \mathbf{1}]} 1 = \sum_{\mathbf{a} \in \mathbf{A}} \prod_{i=1}^n \nu_i(a_i) = \prod_{i=1}^n \sum_{a \in A_i} \nu_i(a).$$

The set of partial derivative operators has equal cardinality:

$$\left| \left\{ \partial_{\mathbf{a}}^{\mathbf{m}}, \mathbf{a} \in \mathbf{A}, \mathbf{m} \in [\mathbf{0}, \nu(\mathbf{a}) - \mathbf{1}] \right\} \right| = \prod_{i=1}^n \sum_{a_i \in A_i} \nu_i(a_i).$$

**Remark 2.** For  $\mathbf{a}, \mathbf{b} \in \mathbf{A}$ , and  $\mathbf{k}, \mathbf{m} \in [\mathbf{0}, \nu(\mathbf{a}) - \mathbf{1}]$  by using the Leibniz derivative rule we easily get:

$$\partial_{\mathbf{a}}^{\mathbf{k}} H_{(\mathbf{b}, \mathbf{m})} = \begin{cases} 0, & \text{if } \mathbf{a} \neq \mathbf{b} \\ 0, & \text{if } \mathbf{a} = \mathbf{b} \text{ and } \mathbf{k} < \mathbf{m} \\ 0, & \text{if } \mathbf{a} = \mathbf{b} \text{ and } \mathbf{k}, \mathbf{m} \text{ are incomparable} \\ 1, & \text{if } \mathbf{a} = \mathbf{b} \text{ and } \mathbf{m} = \mathbf{k} \end{cases}.$$

We now present the Theorem for the uniqueness of the multivariate Hermite interpolating polynomial.

**Theorem 2.1.** *Given the elements  $t_{\mathbf{a}}^{\mathbf{k}} \in \mathbb{K}$ ,  $\mathbf{a} \in \mathbf{A}$ ,  $\mathbf{k} \in [\mathbf{0}, \nu(\mathbf{a}) - \mathbf{1}]$ , there exists a unique  $f \in V(\mathbf{A}, \nu)$  such that  $\partial_{\mathbf{a}}^{\mathbf{m}} f = t_{\mathbf{a}}^{\mathbf{m}}$ ,  $\mathbf{a} \in \mathbf{A}$ ,  $\mathbf{m} \in [\mathbf{0}, \nu(\mathbf{a}) - \mathbf{1}]$ .*

We will derive an expression for the interpolating polynomial  $f$  in Theorem 2.1. First we will use the degree reverse lexicographic order, which will be denoted by  $<$ . More specifically,  $(k_1, \dots, k_n) < (l_1, \dots, l_n)$ , if either of the following holds:

- (i)  $k_1 + \dots + k_n < l_1 + \dots + l_n$ , or
- (ii)  $k_1 + \dots + k_n = l_1 + \dots + l_n$  and  $k_i > l_i$  for the largest  $i$  for which  $k_i \neq l_i$ .

For example, the reverse lexicographic order of the elements in  $[\mathbf{0}, \nu(\mathbf{a}) - \mathbf{1}]$  is

$$\begin{aligned} 1_{\mathbf{a}} : &= (0, \dots, 0) < 2_{\mathbf{a}} := (0, \dots, 0, 1) < 3_{\mathbf{a}} := (0, \dots, 0, 1, 0) < \dots < (n+1)_{\mathbf{a}} := (1, 0, \dots, 0) \\ &< (n+2)_{\mathbf{a}} := (0, \dots, 0, 2) < \dots < (|\nu(\mathbf{a})| - 1)_{\mathbf{a}} := (\nu_1(a_1) - 1, \dots, \nu_n(a_n) - 1). \end{aligned} \quad (2.3)$$

Note that from  $\mathbf{m} \leq \mathbf{n}$  follows  $\mathbf{m} \leq \mathbf{n}$ , and from  $\mathbf{m} < \mathbf{n}$  follows  $\mathbf{m} < \mathbf{n}$ . That means  $\leq$  is a linear extension of  $\leq$ .

The following Theorem provides the closed form of the interpolating polynomial.

**Theorem 2.2.** *The formula of the interpolating polynomial  $f$  is the following*

$$f(\mathbf{x}) := \sum_{\mathbf{a} \in \mathbf{A}} H_{\mathbf{a}}^T \Lambda_{\mathbf{a}}^{-1} T_{\mathbf{a}} = \sum_{\mathbf{a} \in \mathbf{A}} \sum_{i=1}^{|\nu(\mathbf{a})|-1} H_{\mathbf{a}}^T (I_{|\nu(\mathbf{a})|} - \Lambda_{\mathbf{a}})^i T_{\mathbf{a}}, \quad (2.4)$$

where  $H_{\mathbf{a}} = H_{\mathbf{a}}(\mathbf{x})$ ,

$$\Lambda_{\mathbf{a}} = \begin{bmatrix} 1 & 0 & \cdots & 0 & 0 \\ \varepsilon_{2,1} \partial_{\mathbf{a}}^{2_{\mathbf{a}}} H_{(\mathbf{a},1_{\mathbf{a}})} & 1 & \cdots & 0 & 0 \\ \vdots & \vdots & \ddots & \vdots & \vdots \\ \varepsilon_{|\nu(\mathbf{a})|-1,1} \partial_{\mathbf{a}}^{(|\nu(\mathbf{a})|-1)_{\mathbf{a}}} H_{(\mathbf{a},1_{\mathbf{a}})} & \varepsilon_{|\nu(\mathbf{a})|-1,2} \partial_{\mathbf{a}}^{(|\nu(\mathbf{a})|-1)_{\mathbf{a}}} H_{(\mathbf{a},2_{\mathbf{a}})} & \cdots & 1 & 0 \\ \varepsilon_{|\nu(\mathbf{a})|,1} \partial_{\mathbf{a}}^{|\nu(\mathbf{a})|_{\mathbf{a}}} H_{(\mathbf{a},1_{\mathbf{a}})} & \varepsilon_{|\nu(\mathbf{a})|,2} \partial_{\mathbf{a}}^{|\nu(\mathbf{a})|_{\mathbf{a}}} H_{(\mathbf{a},2_{\mathbf{a}})} & \cdots & \varepsilon_{|\nu(\mathbf{a})|,|\nu(\mathbf{a})|-1} \partial_{\mathbf{a}}^{|\nu(\mathbf{a})|_{\mathbf{a}}} H_{(\mathbf{a},(|\nu(\mathbf{a})|-1)_{\mathbf{a}})} & 1 \end{bmatrix}, \quad (2.5)$$

$$x_{\mathbf{a}} = \begin{bmatrix} x_{\mathbf{a}}^{1_{\mathbf{a}}} \\ \vdots \\ x_{\mathbf{a}}^{|\nu(\mathbf{a})|} \end{bmatrix}, T_{\mathbf{a}} = \begin{bmatrix} t_{\mathbf{a}}^{1_{\mathbf{a}}} \\ \vdots \\ t_{\mathbf{a}}^{|\nu(\mathbf{a})|} \end{bmatrix}, H_{\mathbf{a}} = \begin{bmatrix} H_{(\mathbf{a},1_{\mathbf{a}})} \\ \vdots \\ H_{(\mathbf{a},|\nu(\mathbf{a})|)} \end{bmatrix}, |\nu(\mathbf{a})| = \prod_{i=1}^n \nu_i(a_i).$$

In our recent work [1] we also established the  $n$ -dimensional Hermite spline for even, as well as odd number of local support points, which is also referred as stencil, and proved its continuity. Contrary to the most popular convolution-based implementations, the multi-dimensional Hermite interpolant is a non-separable polynomial.

### 3. Hermite spline interpolation Kernel

#### 3.1. Hermite spline interpolation as Convolution and Kernel definition

By considering the application of Theorem 2.2 to a local image neighborhood as a spline, it is easy to observe that the summation in Eq. 2.4 can be thought of as  $n + 1$ -dimensional convolution of image data  $T_{\mathbf{a}}$  with the remaining quantity  $H_{\mathbf{a}}^T \Lambda_{\mathbf{a}}^{-1}$ . Please note that the extra dimension when dealing with  $n$ -dimensional data comes from the use of partial derivatives of the data. The length of this dimension is equal to the cardinality of the reverse lexicographic vectors  $c = \prod_{i=1}^n \nu_i = \nu_0^n$ , where the value of the multiplicity  $\nu(\mathbf{a}) = (\nu_1, \dots, \nu_n) = \nu_0$  is constant for all support points.

Let us further define the notation for the image derivatives for any derivative vector  $\mathbf{k}$ ,  $I_{\mathbf{k}} = I_{k_1, \dots, k_n} = \frac{\partial^{k_1 + \dots + k_n} I}{\partial x_1^{k_1} \dots \partial x_n^{k_n}}$ .

Expressing the interpolation as convolution has the profound advantage of very fast and highly parallelizable execution, especially in parallel architectures such as Graphics Processing Units (GPUs), assuming of course that the convolution Kernel is constant. As with any convolution-based spline interpolation method, the kernel depend on the fractional part of the coordinates where the image values is to be interpolated, in our case  $\mathbf{x}_0 - \lfloor \mathbf{x}_0 \rfloor$ . As in any image or signal interpolation task, the number of support points is equal in each dimension  $|A_1| = \dots, |A_n| = N$ . In certain cases, the fractional part of the required points  $\text{fractional}(x_0) = x_0 - \lfloor x_0 \rfloor$  is constant, or it may only obtain very few specific values. For instance, when generating an intermediate frame in a video sequence, or generating an intermediate slice in a 3D volumetric image, then the fractional part of all required points is constant:  $\text{fractional}(x_0) = [0, 0, 0.5]$ . In the case of zooming into a 2D image by a factor of 2, the fractional parts of the required points are the following:  $[0.5, 0]$ ,  $[0, 0.5]$ , and  $[0.5, 0.5]$ . It is evident that very popular tasks of images and multidimensional signal processing end up as interpolations at points with constant fractional parts.

In such cases, most of the calculations of the proposed Hermite interpolation are repeated. Equivalently, it is possible to express the calculation of the interpolated value as a convolution by an appropriate *constant* kernel. This kernel depends only on the number of support points  $N$  per dimension, the value of the multiplicity function  $\nu$  and the fractional part of  $x_0$ , thus it can be precalculated and used in any image.

In the case of a constant functional part of the coordinates of the required point  $x_0$ ,  $H_{\mathbf{a}} \in \mathbb{R}^{c \times 1}$  is a column with the values for each support point  $\mathbf{a}$ . Thus, the size of  $H_{\mathbf{a}}$  for all support points is  $|A_1| \times \dots \times |A_n| \times c$ . The calculation of the values of  $H_{\mathbf{a}}$  is performed only once: given the local support points, the coefficients of the univariate polynomials  $H_{a_i}(x_i)$  are stored in an array of dimensions  $|A_1| \times \dots \times |A_n| \times c \times n \times \deg_i$ . An efficient computational implementation of

Hermite splines lies in the construction of convolution kernels using the formulas (2.5). The lower triangular matrices are of dimension  $N_1 \times \dots \times N_n \times c \times c$  can be pre-calculated and inverted  $\Lambda_{\mathbf{a}}^{-1}$ .

According to the definition of the convolution operator, the kernel needs to be mirrored with respect to its center. Thus, we can construct a tensor  $K$  of size  $N_1 \times \dots \times N_n \times c$  that will be used as a convolution kernel, as follows:

$$K(i_1, \dots, i_n, :) = \underbrace{H_{(N_1-i_1+1, \dots, N_n-i_n+1, :)}^T}_{1 \times c} \underbrace{\Lambda_{(N_1-i_1+1, \dots, N_n-i_n+1, :, :)}^{-1}}_{c \times c}.$$

In the above we used the tensor notation  $X_{i,j,:}$  where  $:$  denotes the elements with any value of the corresponding index. The flipping of the indices except the last one is necessary to implement the calculations as a series of  $n$ -dimensional convolution operations (considering  $c$   $n$ -dimensional Hermite kernels. If Hermite kernels are considered as one  $n+1$ -dimensional, the convolution is implemented in  $n+1$ -dimensions flipping the last index as well. If the operation of correlation can also be performed efficiently, then there is no need for index flipping:

$$K(i_1, \dots, i_n, :) = H_{(i_1, \dots, i_n, :)}^T \Lambda_{(i_1, \dots, i_n, :, :)}^{-1}.$$

Let us consider the 3D case:  $n = 3$ , where the grid points are triplets:  $\mathbf{a} = (i, j, k)$  and  $|A_1|$ .

$$K(i, j, k, :) = H_{(N_1-i+1, N_2-j+1, N_3-k+1, :)}^T \Lambda_{(N_1-i+1, N_2-j+1, N_3-k+1, :, :)}^{-1}$$

Given the complicated nature of Hermite splines, we have prepared and illustrated the procedural steps and the structural components required to apply Hermite kernels to 2D and 3D images, as depicted in Fig. 2 and Fig. 3, respectively. Therefore, having constructed the Hermite Kernels, we present the algorithmic steps and the data structures of applying Hermite kernels in Fig. 2 and Fig. 3 for 2D and 3D images respectively, using data derivatives.

As an example, assuming that  $v(\mathbf{a}) = 2$  for any grid point, equivalently all combinations of up to 1st order derivatives are concerned, consequently, the cardinality  $c = 4$ . If i.e. we choose to use  $N_1 = N_2 = 5$  support points along each axis, the resulting Hermite kernel  $K^H$  of size  $5 \times 5 \times 4$ . This is a 3rd order tensor which can also be treated as a series of 4 2D kernels, each of size  $5 \times 5$ . In the case of  $v(\mathbf{a}) = 3$  the kernel size becomes  $5 \times 5 \times 8$ . Fig. 1 shows the first 4 slices of the corresponding Hermite kernel for interpolating images at  $(0.5, 0.5)$  with respect to each pixel.

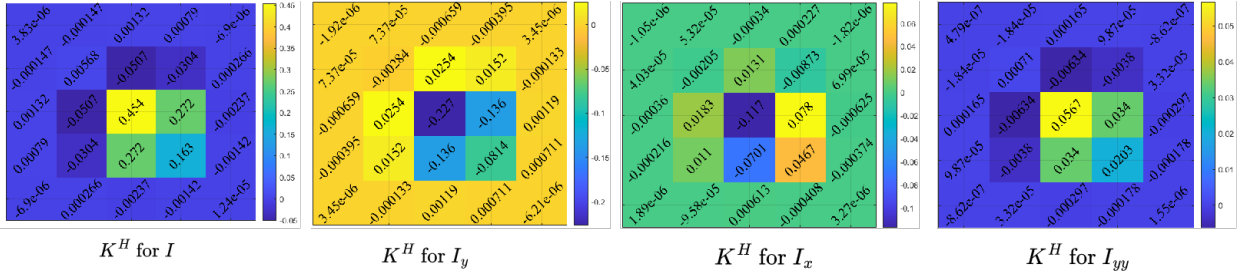


Figure 1: Numerical values for 2D Hermite spline interpolation for x2image zooming. The first 4 (out of 8) kernels are shown corresponding to approximated image partial derivatives up to 1st order ( $v = 2$ ).

### 3.2. Hermite interpolation Convolution for FIR-based numerically approximated data derivatives

In the most frequent case of signal and image/video processing, the values of the derivatives are numerically approximated, using Finite impulse response (FIR) kernels, or Infinite impulse response (IIR), as described in [11]. Assuming the use of FIR kernels, it becomes possible to combine the FIR derivative kernels with the derived Hermite kernels into a single kernel with dimensionality equal to the dimensionality of the given data. More specifically, let us define the derivative kernel  $G_{\mathbf{k}}$  that performs the image derivative approximation defined in vector  $\mathbf{k}$ ,  $G_{\mathbf{k}} * I = I_{\mathbf{k}} = I_{k_1, \dots, k_n} = \frac{\partial^{k_1 + \dots + k_n} I}{\partial x_1^{k_1} \dots \partial x_n^{k_n}}$ . For instance,  $G_{02}$  is the kernel that approximate image derivatives of the 2nd order along the

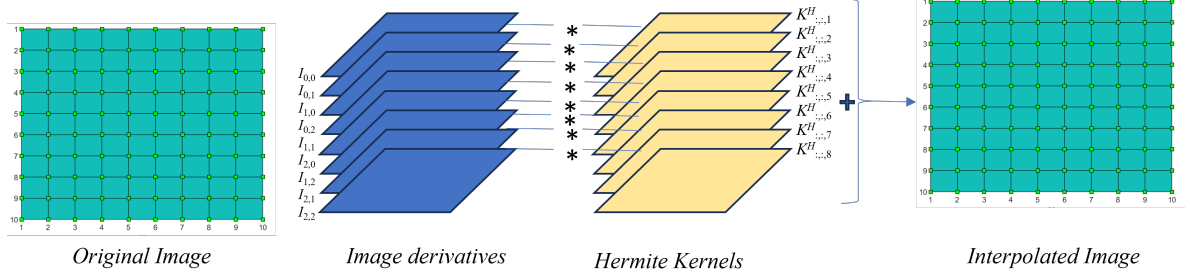


Figure 2: Diagram of convolution-based 2D Hermite spline interpolation with approximated image partial derivatives up to 1st order ( $v = 2$ ).

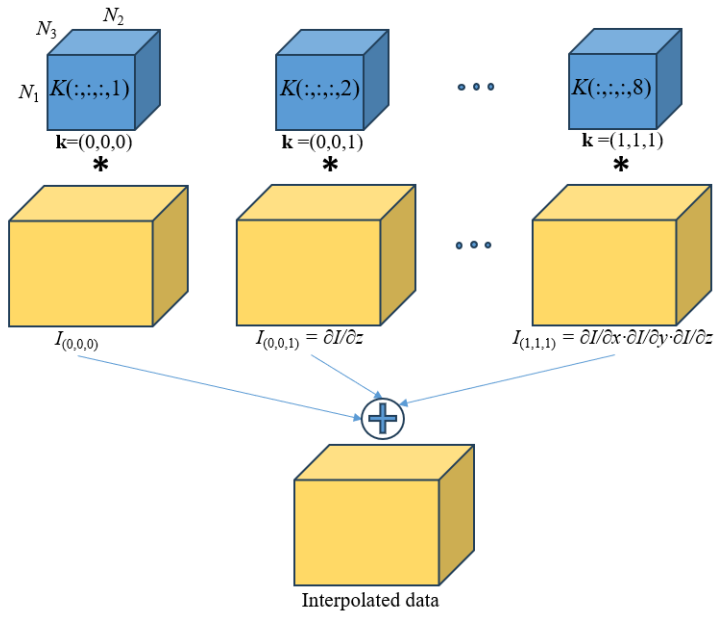


Figure 3: Diagram of convolution-based 3D Hermite spline interpolation with approximated image partial derivatives up to 1st order ( $v = 2$ ).

columns. Obviously, when  $\mathbf{k} = \mathbf{0}$ , then  $G = [1]$  is the discrete Dirac function. The single  $n$ -dimensional Hermite Kernel that combines all partial derivatives of the given data is as follows:

$$\mathcal{K} = \sum_{j=1}^c G_{\mathbf{k}_j} * K(:, \dots, :, j),$$

where  $\mathbf{k}_j$  refers to the reverse lexicographic order of the elements in  $[\mathbf{0}, v(\mathbf{a}) - 1]$  according to relation 2.3,  $\mathbf{k}_j = j_{\mathbf{a}}$ .

Let us consider a practical example of Hermite coordinate interpolation, applied to 2D images ( $n = 2$ ) and considering derivatives up to 1st degree  $v(\mathbf{a}) = (2, 2)$  for any  $\mathbf{a}$ . The cardinality of the reverse lexicographic vectors is  $c = 4$ , thus produces four (4) derivative vectors, according to [11]:  $\mathbf{k}_1 = (0, 0)$ ,  $\mathbf{k}_2 = (0, 1)$ ,  $\mathbf{k}_3 = (1, 0)$ ,  $\mathbf{k}_4 = (1, 1)$ . The corresponding FIR derivative kernels, generated according to [11] are  $G_{00}$ ,  $G_{01}$ ,  $G_{10}$  and  $G_{11}$ . It should be mentioned that  $G_{00} = (1)$ ,  $G_{01} \in \mathbb{R}^{q \times 1}$ ,  $G_{10} = G_{01}^T$  and  $G_{11}$  is approximated as  $G_{10} * G_{01}$ .

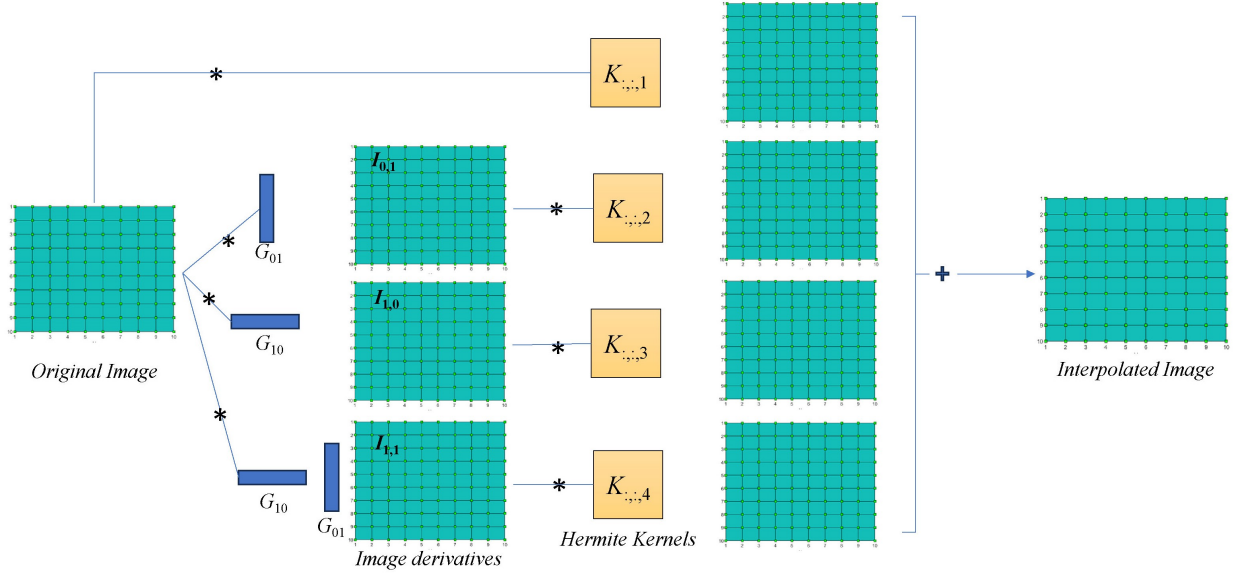


Figure 4: Diagram of applying Hermite spline interpolation on 2D image.

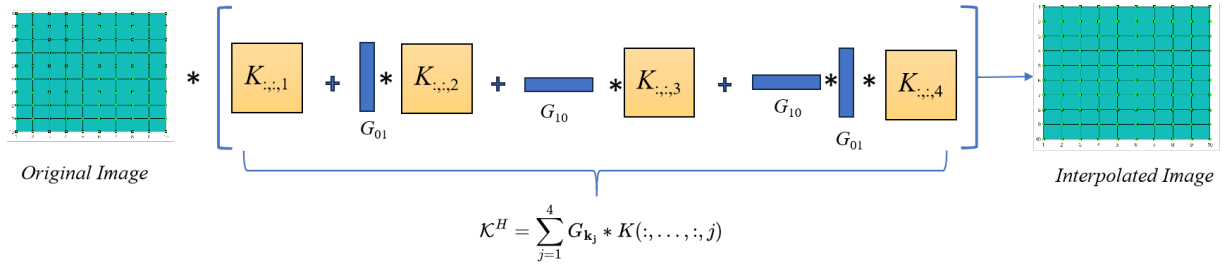


Figure 5: Principles of constructing a single 2D kernel that includes all 2D Hermite kernels, as well as the FIR differentiating kernels.

### 3.3. Hermite interpolation Convolution for numerically approximated data derivatives using IIR

A rather more complicated method to approximate signal and image derivatives is the implicit derivatives. As proposed by [6] for signals and implemented by [7] for images, this method estimates derivatives implicitly:

$$Q_1 * f^{(1)} = R_1 * f$$

$$Q_2 * f^{(2)} = R_2 * f$$

where  $Q_1, Q_2$  are  $5 \times 1$  symmetric kernels and  $R_1, R_2$  are  $7 \times 1$  antisymmetric and symmetric kernels respectively. The elements of each kernel is provided in [6]. In [11] the implementation of implicit derivatives is based on a cascade of two IIR filters: a causal and an anti-causal one with appropriate initial conditions and poles (roots of the denominator of the filters' transfer functions) that are pairs of reciprocals. The application to images is performed column-wise and then row-wise in a very efficient manner. This process is shown in the diagram of Fig. 6. As it will be shown in the results, IIR-based image derivatives produce better Hermite interpolation compared to simpler FIR filters.

### 3.4. Convolution-based implementation of 2d Image Super Resolution

Let us consider the case of 2D image scaling by integer factor  $s$ . In the special case of  $s = 2$ , then for each given image pixel  $(i, j) = (x, y)$ , the new image values have to be computed at three new locations:  $(x + 0.5, y)$ ,  $(x, y +$

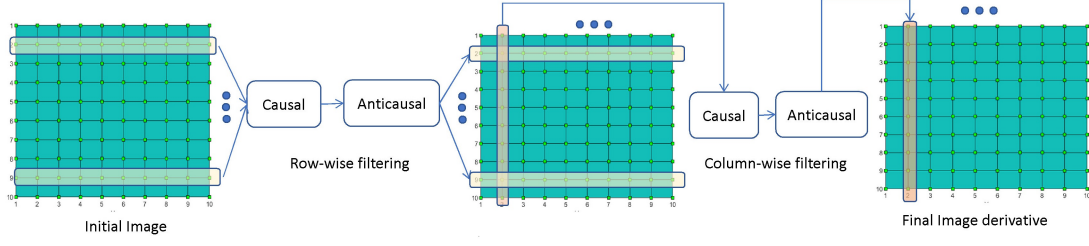


Figure 6: The steps of IIR-based implicit image derivative approximation.

0.5),  $(x + 0.5, y + 0.5)$ , or equivalently the value to the right of the current pixel, down and right-down of the current pixel, respectively. This can be achieved most efficiently by constructing three different kernels:  $K^{HR}$ ,  $K^{HD}$ ,  $K^{HRD}$  and convolving the image with each one to generate the values at the corresponding pixels. Figure 7 depicts this process graphically using green squares for the given pixels and red, blue and yellow circles for the east, south and south-east pixels, respectively. This is a generic approach, applicable to any convolution-based method and it is considered computationally very efficient, since image convolution operations are very efficiently implemented and highly parallelizable.

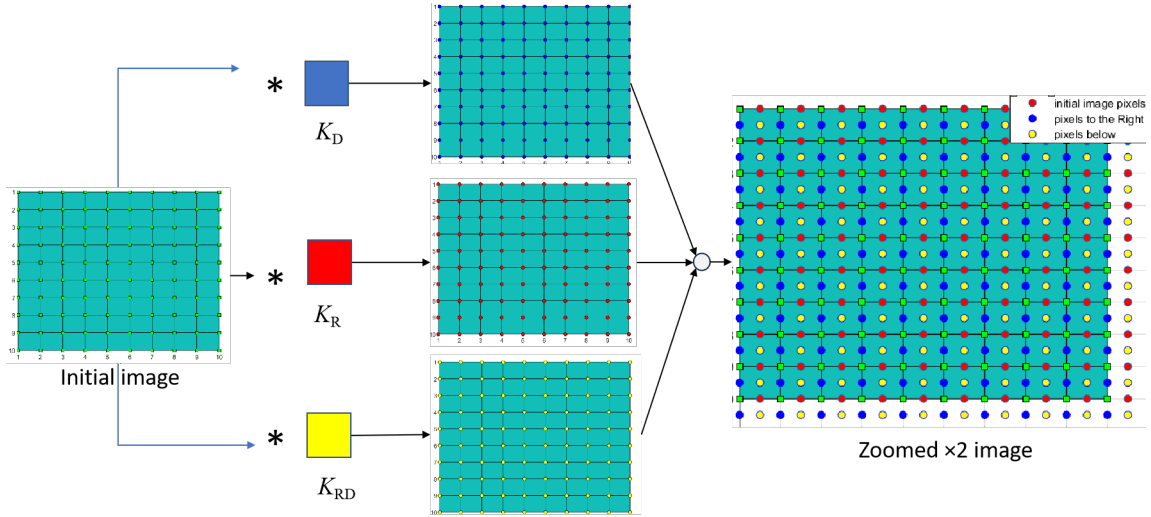


Figure 7: Using 3 constant kernels to implement 2D image zoom x2.

### 3.5. Generic framework for the evaluation of interpolation methods

We implemented a straightforward framework for the evaluation of interpolation methods on a large number of images, that has already been used in many works for this purpose. For any given image, the lines and columns (and slices in case of 3D images) are decimated, e.g. by removing the one every few of them (skip factor  $s_k$ ). Obviously, the scale factor is given by  $s = \frac{1}{s_k + 1}$ . Before this step, a low-pass (LP) smoothing filtering should be applied to alleviate the introduction of frequency aliasing. The normalized cut-off frequency of this filter should be chosen equal to the reciprocal of the scale factor  $\omega_c = \pi \frac{1}{s}$  (assuming sampled frequency range  $[-\pi, \pi]$ ). The interpolation methods are applied on the decimated image to generate an image of the original dimensions. An ideal interpolation would produce an image identical with the original. In order to exaggerate the differences between interpolation methods the previous steps are applied in a number of cascaded repetitions (using the interpolated image as the source for the next subsampling), thus generating an incremental error. The aforementioned steps are shown graphically in Fig. 8.



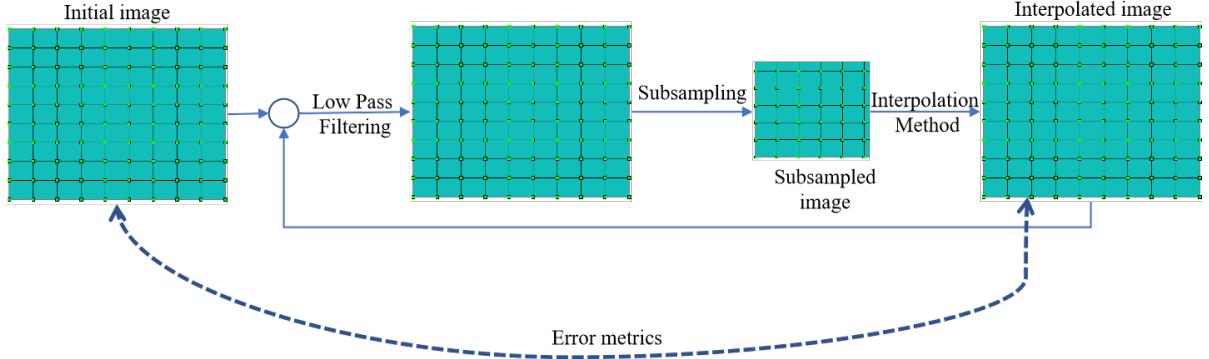


Figure 8: Scheme for quantitative evaluation of image zooming using multiple repetitions.

#### 4. Results

The baseline for image interpolation is usually considered as the nearest neighbor one (expected to be the worst performer). Bilinear and bicubic interpolation are also convolution based methods that are also included in this work as base lines. In addition, we employed generalized convolution methods, which are considered state-of-the-art between the convolution-based methods. More specifically, the generalized convolution methods are using a pre-filtering step which consists of a number of pairs of causal and anti-causal filterings, each with reciprocal roots. We employed the best performing of these methods, namely b-spline [4], [5] and maximal order minimal support (oMOM) up to the 5th degree (MOM4, MOM5) [3]. Finally, we included deep learning (DL) methods in the comparison. More specifically, we used the opencv implementation of three super-resolution neural networks with convolutional and deconvolutional layers, that generate zoomed versions of their input images, provided as already pretrained: ESPCN [8] FSRCNN [9] LapSRN [10]. In terms of the proposed Hermite spline kernels, we experimented with  $N_1 = N_2 = 5$  support points along each axis, and  $\nu = 3$  resulting in Hermite kernels  $K^H$  of size  $5 \times 5 \times 9$  ( $c = 4$ ). The image partial derivatives up to 2nd order are approximated using 3, 5 and 7-point FIR filters, as well as IIR filters.

We utilized well established error metrics between the original image and the zoomed (after subsampling): PSNR, expressed in db (with greater values being better) and the Structural similarity index measure [13] -SSIM. SSIM is a perception-based model that considers image degradation, including both luminance masking and contrast masking terms. The maximum value of 1 to indicate best interpolation quality.

Results are presented in the case of 20 standard images, which have been benchmarks in image processing [14], shown in Fig. 9.

Figure 10 shows the achieved SSIM by proposed Hermite with IIR image derivatives, the b-spline deg 5, two deep learning approaches, and the bilinear as baseline method for the Barbara image. In Figure 10, while both the b-spline a deg 5 and the proposed Hermite method with IIR image derivatives exhibit superior performance, it's noteworthy that the Hermite method achieves a slight edge over the b-spline. The bilinear deteriorates very rapidly as the cascaded repetitions increase. The two deep learning methods also deteriorate significantly more than the best performers with increasing repetitions. A similar result is shown in Fig. 11 in terms of PSNR for the same image. In this case, the deep learning methods appear to deteriorate more slowly, seemingly converging with the best performers beyond the 20 repetitions. However, a visual inspection of the interpolated images in Figure 13 and 14 indicates that the blurring induced by the methods is very apparent. The high PSNR values are due to smaller errors in the flat image areas, whereas the fine image details are not preserved. Figure 12 shows average PSNR form all 20 images achieved by the proposed Hermite with FIR 7-point image derivatives and 5 more generalized convolution methods. The proposed Hermite spline method marginally outperforms the rest of the methods.

Detailed numeric results for each image and each of the methods are shown in Table 1 and Table 2, after the 20 repetitions. Color is used to highlight the methods that yield the best results for each image. It can be observed that the proposed Hermite with 7-point FIR image derivatives achieves the highest PSNR in 16 out of 20 images (with oMOM deg 5 and Deep Learning LapSRN achieving best PSNR in 2 images). In terms of SSIM, the Hermite with IIR image derivatives achieved the best performance in 17 out of 20 images, with the oMOM deg 5 being the best method

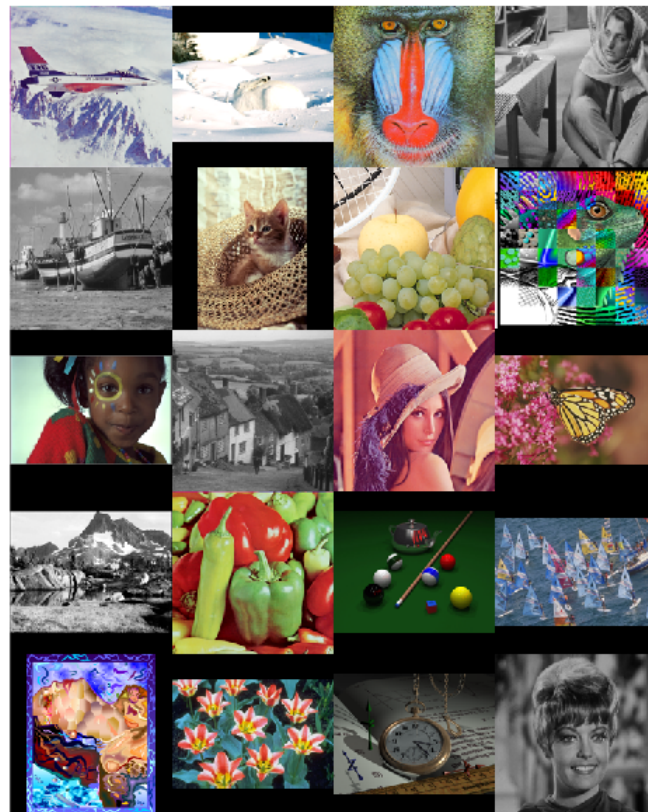


Figure 9: The dataset of the standard 20 images used for evaluation.

in 3 (out of 20) images and 1 image in tie between the two aforementioned methods.

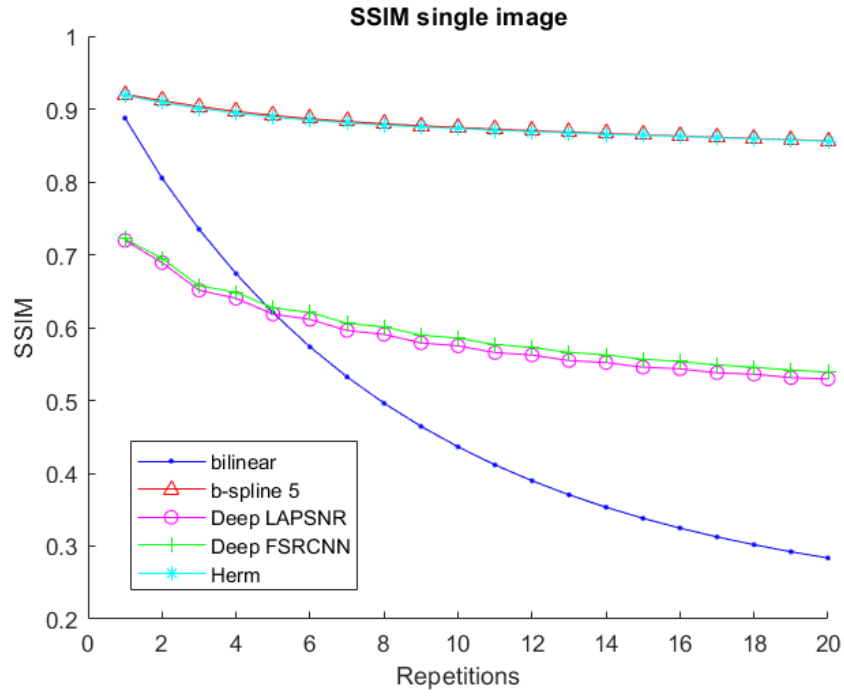


Figure 10: SSIM achieved by the methods in comparison for the Barbara image, using multiple repetitions of image zooming.

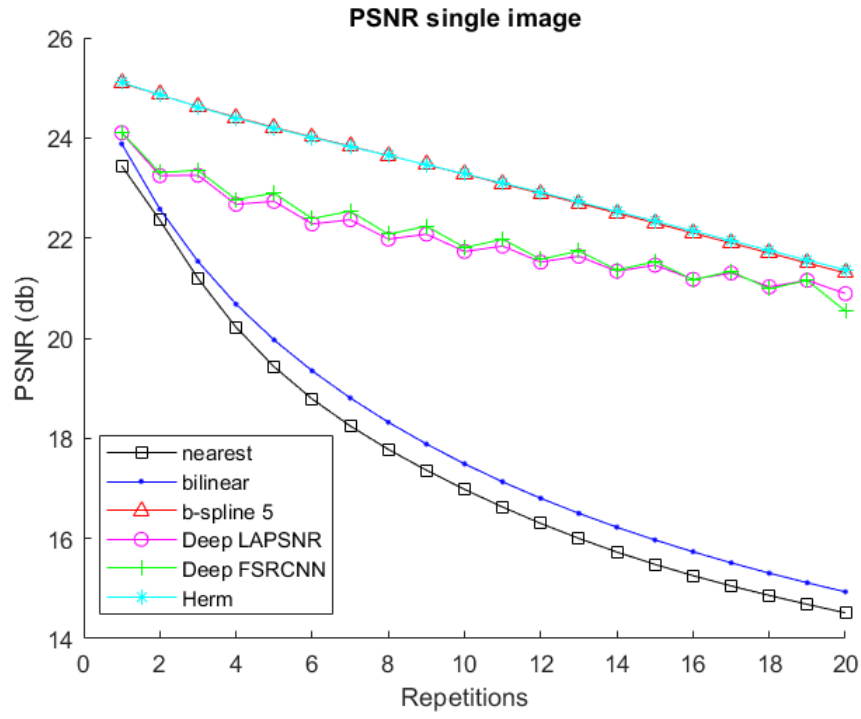


Figure 11: PSNR achieved by the methods in comparison for the barbara image using multiple repetitions of zooming.

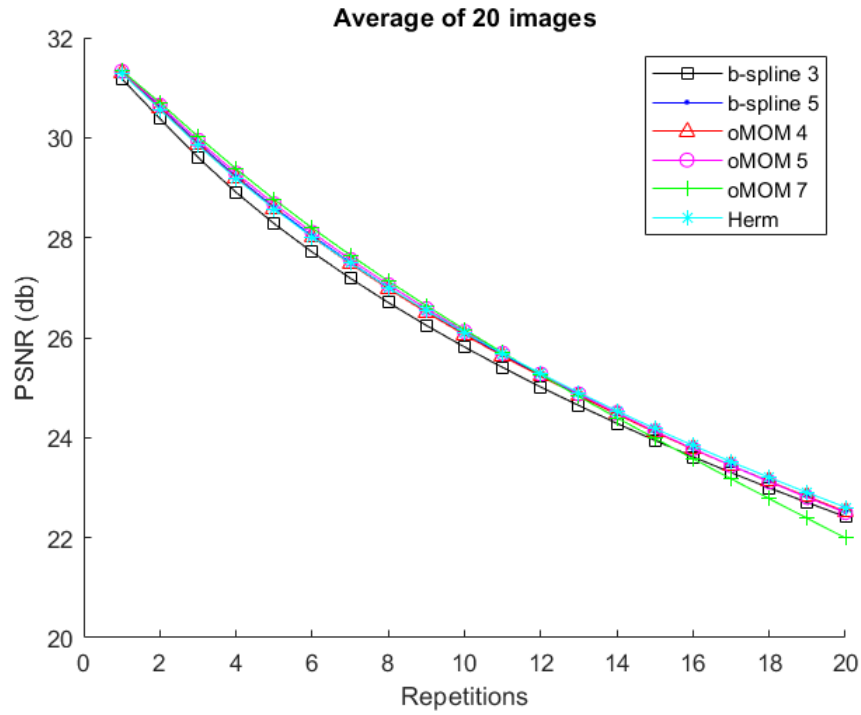


Figure 12: Average PSNR over all images for the best performing methods, using multiple repetitions of image zooming.

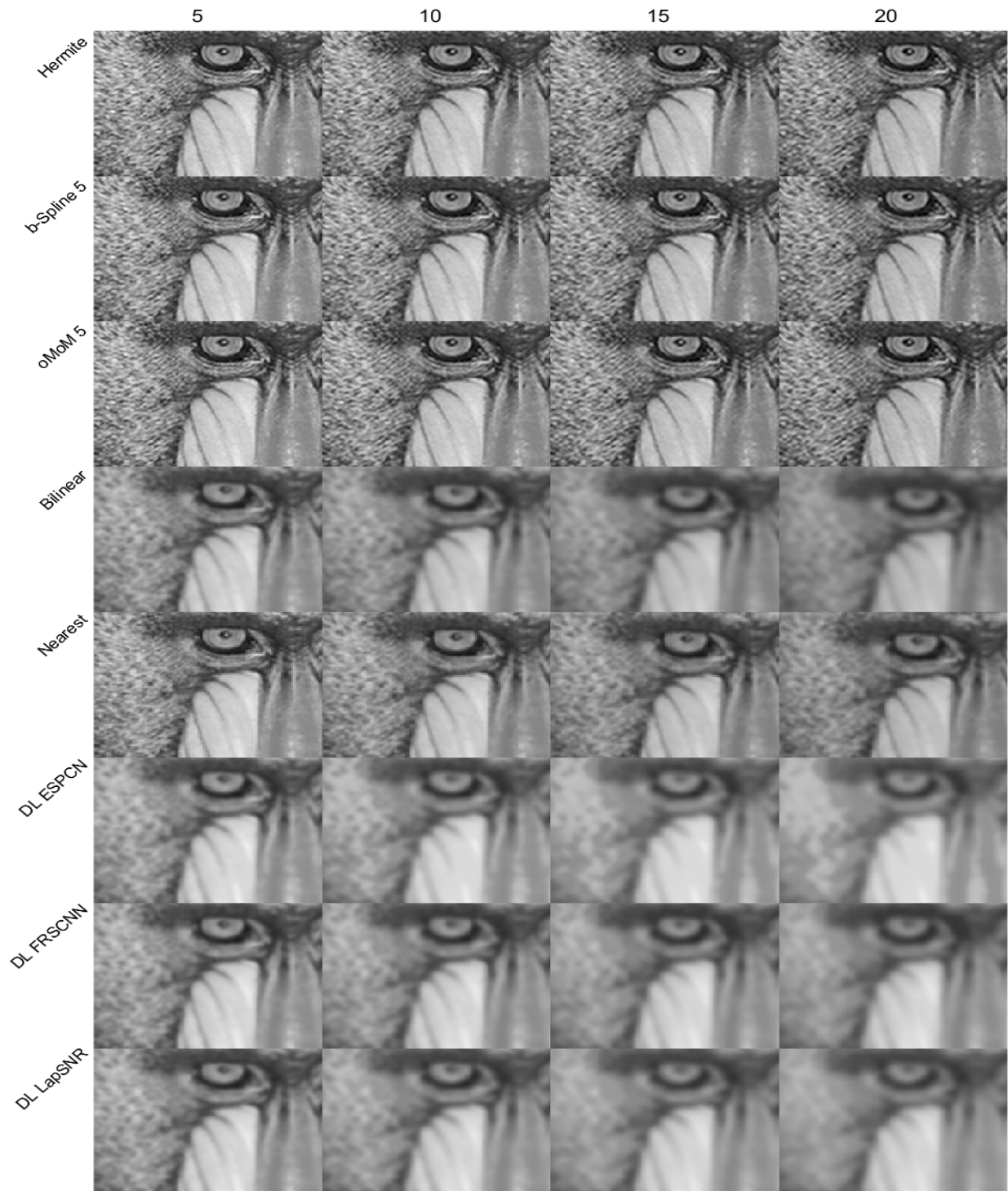


Figure 13: A cropped region from the 4th image (Baboon) interpolated by several methods, for 5, 10, 15 and 20 repetitions of the 2x zoom in and out operator.



Figure 14: A cropped region from the 4th image (Barbara) interpolated by several methods, for 5, 10, 15 and 20 repetitions of the 2x zoom in and out operator.

Table 1: PSNR achieved by all methods under comparison for each image, after 20 repetitions (best values indicate in color).

Image	Kernel Based			Generalized Convolution					Deep Learning			Hermite		
	Nearest	Bilinear	Bicubic	B-Spline 3	B-Spline 5	oMOM 4	oMOM 5	LAPSNR	ESPCN	FSRCNN	FIR 7	FIR 5	FIR 3	IIR
airplane	13.9789	14.5733	16.2826	20.7689	20.7242	20.7450	20.6338	20.7452	19.9487	20.3019	20.8902	20.4785	20.4138	20.3029
artichare	16.1653	16.5568	17.8573	20.3521	20.2744	20.2902	20.2138	21.6732	20.3223	20.8963	20.3849	19.9625	19.9483	19.8919
baboon	15.6938	16.0674	16.8692	19.6032	19.7959	19.7844	19.8090	19.5492	19.1706	19.3805	19.8364	19.5891	19.4487	19.7227
barbara	14.6830	15.1143	17.7198	21.4615	21.5012	21.5031	21.4852	20.8910	20.5493	20.8196	21.5577	21.3387	21.2847	21.3589
boat	15.8791	16.3873	18.2344	23.0309	23.1686	23.1664	23.1520	21.3695	20.6271	21.2596	23.2581	22.8891	22.7563	22.9847
cat	14.9593	15.5389	16.4353	22.1417	22.2904	22.2886	22.2753	19.2665	19.0057	19.1999	22.4049	21.9933	21.8461	22.1147
fruits	16.9229	17.3626	18.9296	22.0392	22.0816	22.0861	22.0532	22.5253	21.6861	22.1928	22.1818	21.7774	21.7026	21.8262
frymire	10.3165	10.8214	12.0235	16.8943	17.2887	17.2556	17.3614	14.1494	14.1640	14.2916	17.2737	17.0492	16.8125	17.3562
girl	16.3423	16.6693	19.5499	23.9752	24.0209	24.0221	24.0039	23.2041	22.6643	23.1637	24.0732	23.6959	23.6415	23.5875
goldhill	17.0245	17.6263	18.8161	23.6368	23.6799	23.6879	23.6381	23.4340	22.7654	23.0888	23.8308	23.4709	23.3702	23.5270
lena	15.5165	15.9859	18.7920	23.9165	23.9649	23.9707	23.9273	22.7220	21.9453	22.4613	24.0607	23.6572	23.5728	23.6590
monarch	15.4562	16.1737	16.3694	24.2650	24.4881	24.4764	24.5002	20.6106	20.3271	20.6611	24.5432	24.1614	23.9954	24.3238
mountain	11.5181	12.2248	13.6800	17.6614	17.7525	17.7580	17.7084	15.8753	15.7709	15.8742	17.8573	17.6761	17.5627	17.4953
peppers	13.8670	14.4778	17.5851	23.4312	23.3051	23.3410	23.1631	21.9124	21.3532	21.7376	23.5345	23.1509	23.1009	22.6973
pool	20.1182	20.6315	24.3089	30.9274	31.1676	31.1547	31.1818	27.0699	27.0729	26.9579	31.2178	30.8301	30.6582	30.9388
sails	16.0689	16.6202	17.6804	22.7821	23.0652	23.0464	23.0964	20.9101	20.4932	20.7882	23.0973	22.7621	22.5709	22.9584
serrano	13.2700	13.9410	15.2754	21.7259	21.9337	21.9187	21.9629	18.6987	18.5713	18.8536	21.9400	21.6286	21.4992	21.5797
tulips	14.2728	14.7993	17.0047	24.2568	24.4460	24.4359	24.4586	21.7958	21.4981	22.0677	24.4879	24.0866	23.9499	24.2048
watch	19.0952	19.6250	20.5156	26.9449	27.1997	27.1837	27.2256	23.9174	23.4855	23.5796	27.2251	26.8505	26.6781	27.0079
zelda	15.9276	16.3474	19.3039	24.2378	24.2499	24.2571	24.2140	26.6032	15.4213	25.8155	24.3450	23.9444	23.8865	23.9349



Table 2: SSIM achieved by all methods under comparison for each image, after 20 repetitions (best values indicate in color).

Image	Kernel Based			Generalized Convolution					Deep Learning			Hermite		
	Bilinear	Bicubic	B-Spline 3	B-Spline 5	oMOM 4	oMOM 5	LAPSNR	ESPCN	FSRCNN	FIR 7	FIR 5	FIR 3	IIR	
airplane	0.4699	0.5754	0.9580	0.9654	0.9649	0.9661	0.6872	0.6775	0.6886	0.9658	0.9618	0.9564	0.9669	
artichare	0.5852	0.6852	0.9741	0.9785	0.9783	0.9788	0.8031	0.7804	0.7985	0.9790	0.9762	0.9728	0.9791	
baboon	0.2083	0.2861	0.8189	0.8552	0.8526	0.8607	0.2893	0.2889	0.2961	0.8547	0.8427	0.8210	0.8643	
barbara	0.2923	0.4816	0.8468	0.8578	0.8569	0.8597	0.5294	0.5273	0.5387	0.8572	0.8523	0.8456	0.8604	
boat	0.3255	0.4389	0.9171	0.9342	0.9330	0.9368	0.5232	0.5202	0.5321	0.9336	0.9267	0.9157	0.9380	
cat	0.2320	0.3761	0.9470	0.9587	0.9579	0.9602	0.4857	0.4794	0.4989	0.9585	0.9540	0.9465	0.9606	
fruits	0.5156	0.6257	0.9396	0.9495	0.9487	0.9511	0.6958	0.6857	0.6975	0.9491	0.9443	0.9379	0.9518	
frymire	0.1086	0.4033	0.9609	0.9710	0.9702	0.9728	0.3643	0.3569	0.3627	0.9705	0.9656	0.9594	0.9733	
girl	0.6220	0.6892	0.9354	0.9457	0.9450	0.9474	0.7121	0.7027	0.7098	0.9455	0.9409	0.9343	0.9479	
goldhill	0.3034	0.4034	0.9211	0.9370	0.9359	0.9393	0.5373	0.5344	0.5419	0.9368	0.9307	0.9205	0.9403	
lena	0.4116	0.6100	0.9532	0.9613	0.9608	0.9625	0.6811	0.6733	0.6856	0.9611	0.9572	0.9517	0.9626	
monarch	0.4758	0.5498	0.9671	0.9723	0.9719	0.9731	0.7231	0.7189	0.7301	0.9721	0.9691	0.9656	0.9731	
mountain	0.1993	0.2880	0.8380	0.8643	0.8624	0.8683	0.2770	0.2702	0.2790	0.8645	0.8547	0.8383	0.8710	
peppers	0.4467	0.6239	0.9604	0.9652	0.9648	0.9658	0.6838	0.6782	0.6930	0.9651	0.9619	0.9584	0.9656	
pool	0.8076	0.8779	0.9588	0.9620	0.9617	0.9626	0.8987	0.8914	0.8942	0.9616	0.9585	0.9557	0.9623	
sails	0.1967	0.2845	0.8691	0.8967	0.8947	0.9010	0.3681	0.3672	0.3740	0.8959	0.8860	0.8690	0.9036	
serrano	0.2520	0.3781	0.9408	0.9500	0.9493	0.9516	0.5472	0.5411	0.5556	0.9492	0.9442	0.9380	0.9516	
tulips	0.2354	0.4224	0.9460	0.9570	0.9562	0.9587	0.5855	0.5769	0.5992	0.9564	0.9512	0.9440	0.9591	
watch	0.4952	0.5728	0.9777	0.9821	0.9818	0.9828	0.7243	0.7209	0.7213	0.9819	0.9794	0.9764	0.9824	
zelda	0.4670	0.6567	0.9680	0.9731	0.9728	0.9738	0.7722	0.7615	0.7729	0.9730	0.9703	0.9670	0.9735	



## 5. Conclusions and further work

In this work we proposed the construction of Hermite kernels for 2D image interpolation, based on the Hermite splines that were defined and studied on  $n$ -dimensional grid [1]. This formulation makes the Hermite splines easy to implement. In this work we also calculated the kernels for 2D image zooming and perform comparisons with many state-of-the-art methods for 20 images. The obtained results reveal several interesting aspects. The generalized convolution methods achieved very good results both in terms of PSNR and SSIM. The convolution methods were inferior. The proposed Hermite kernels outperformed almost all methods in the majority of the 20 images, up to 20 repetitions of the zoom in and out operator. The Deep learning based methods exhibited an increasing blurring as the number of repetitions increased. However the resulting PSNR appeared disproportionally high. This is due to small MSE (mean square error), due to small errors in relatively flat areas, despite the apparent loss of spatial resolution in areas with fine detail. The SSIM error metric was low, since, as expected, it was sensitive to this issue. Future work will investigate similar tasks in 3d images or videos.

## References

- [1] A. I. Kechriniotis, K. K. Delibasis, I. P. Oikonomou, and G. N. Tsigaridas. Classical multivariate Hermite coordinate interpolation on  $n$ -dimensional grids. arXiv:2301.01833 [math.NA], 2023.
- [2] K. K. Delibasis and A. Kechriniotis. A new formula for bivariate Hermite interpolation on variable step grids and its application to image interpolation. *IEEE Transactions on Image Processing*, 23(7):2892–2904, 2014. doi:10.1109/TIP.2014.2322441.
- [3] T. Blu, P. Thévenaz, and M. Unser. MOMS: Maximal-order interpolation of minimal support. *IEEE Transactions on Image Processing*, 10(7):1069–1080, 2001.
- [4] M. Unser, A. Aldroubi, and M. Eden. B-spline signal processing. I. Theory. *IEEE Transactions on Signal Processing*, 41(2):821–833, 1993.
- [5] M. Unser, A. Aldroubi, and M. Eden. B-spline signal processing. II. Efficiency design and applications. *IEEE Transactions on Signal Processing*, 41(2):834–848, 1993.
- [6] S. K. Lele. Compact finite difference schemes with spectral-like resolution. *Journal of Computational Physics*, 103(1):16–42, 1992.
- [7] A. Belyaev. On implicit image derivatives and their applications. *Journal of Computational Physics*, 103:16–42, 1992.
- [8] W. Shi, J. Caballero, F. Huszár, J. Totz, A. Aitken, R. Bishop, D. Rueckert, and Z. Wang. Real-Time Single Image and Video Super-Resolution Using an Efficient Sub-Pixel Convolutional Neural Network. *Proceedings of the IEEE Conference on Computer Vision and Pattern Recognition (CVPR)*, pages 1874–1883, 2016.
- [9] C. Dong, C. C. Loy, and X. Tang. Accelerating the Super-Resolution Convolutional Neural Network. *Proceedings of European Conference on Computer Vision (ECCV)*, pages 1–17, 2016.
- [10] W.-S. Lai, J.-B. Huang, N. Ahuja, and M.-H. Yang. Deep laplacian pyramid networks for fast and accurate super-resolution. *Proceedings of the IEEE Conference on Computer Vision and Pattern Recognition (CVPR)*, pages 5835–5843, 2017.
- [11] K. K. Delibasis, A. Kechriniotis, and I. Maglogiannis. On centered and compact signal and image derivatives for feature extraction. *Artificial Intelligence Applications and Innovations: 9th IFIP WG 12.5 International Conference, AIAI 2013, Paphos, Cyprus, September 30–October 2, 2013, Proceedings 9*, pages 318–327, 2013, Springer.
- [12] K. Delibasis, A. Kechriniotis, and N. Assimakis. New closed formula for the univariate Hermite interpolating polynomial of total degree and its application in medical image slice interpolation. *IEEE Transactions on Signal Processing*, 60(12):6294–6304, 2012, IEEE.
- [13] B. Debnath. SSIM-Map calculation of an image in Python, 2023. Available at: <https://github.com/BiswarupDebnath/SSIM-Map>
- [14] Semnan University AI. Image Processing Benchmark - A collection of standard test images. GitHub repository, GitHub, 2024. Available at: <https://github.com/semnan-university-ai/image-processing-benchmark/>. The latest commit hash here.